Compact Interferometric Antenna Array for UWB Direction Finding

Pietro Bia*(1), Alessandro Calcaterra(1), Domenico Gaetano(1), Christian Canestri(1), Riccardo Ardoino(1), Luca Scorrano(1) and Antonio Manna(1)
(1) Elettronica S.p.A., Roma, Italy,

Abstract

In this paper, a novel interferometer system for direction of arrival (DoA) estimation is presented. The design provides an extremely compact and lightweight interferometric panel that operates in an ultra-wideband (UWB) frequency range, from 2 GHz to 18 GHz. Two sets of sinuous antennas have been designed to properly manage the frequency spectrum of interest.
In order to guarantee the detection of the majority of impinging waves, both sets of antennas work with a slant 45 (S45) polarization, ensuring good matching properties, high level of cross polarization isolation and stable radiation patterns.
The design layout has been implemented to achieve an extremely compact structure maintaining a controlled phase error on each radiating element. Advantages in terms of size, weight and cost have been also presented. The complete interferometer structure has been manufactured and measured. Finally, a DoA estimation has been evaluated considering the measured patterns.

1 Introduction

The main characteristic of an interferometer system is to determine the DoA of interesting signals minimizing the angular error [1, 2]. An appropriate determination of DoA is then of particular importance in many applications, both civil and military. The DoA is found by elaborating signals detected by antennas that are conveniently displaced on the considered platform. This structure is called interferometer, and distances between radiating elements play a key role in ambiguity resolution and level of accuracy [3, 4]. Moreover, antenna patterns need to be as more stable as possible in frequency and guarantee wide beams (usually greater than 90 degrees on the azimuthal plane). A radiating element that is particularly suitable for these kind of applications is the sinuous antenna. It is a very appealing and versatile ultra-wideband (UWB) radiating element that was firstly introduced and patented by DuHamel in 1987 [5]. In literature, there are several example of this antenna, used both in its dipole and slot versions, with two or four arms [6–11]. The basic sinuous antenna shape satisfies the self-complementary principle, providing uncommonly stable patterns along the whole frequency band. It is usually printed on a planar circuit, exploiting the high simplicity of this manufacturing technique. Therefore, considering the fundamental mode, it radiates a dual-lobe pattern. In order to radiate a single lobe pattern, a proper cavity with radio-frequency absorber have been implemented. The excitation of the fundamental mode is provided by a printed circuit balun, that is designed to guarantee a balanced current on the circuit branches. The Klopfenstein balun [12] has been adopted as feeding circuit and mounted orthogonally to the antenna. Due to the frequency-dependent length, the balun is responsible of the total height of the cavity. Generally, in a receiving system, incoming waves have unknown DoA and polarization. The sensitivity of the interferometer is a fundamental parameter, and it is obviously related to the necessity of intercept any possible polarization for this reason the proposed sinuous antennas have been designed with a S45 polarization. The frequency band of interest is from 2 GHz to 18 GHz, that is more than 3 octaves of frequency band,. To cover this UWB frequency band, the idea has been to design two sets of sinuous antennas, the first set optimized from 2 GHz to 6 GHz (low band - LB) and the second from 6 GHz to 18 GHz (high band - HB).

2 Sinuous Antennas Design and Manufacturing

In this section, brief description of the two radiating elements (LB and HB) that compose the interferometer has been done.
The sinuous profile is obtained by the following equation:

$$\phi(r) = (-1)^{-1}\alpha \sin\left(\frac{\pi\, log\left(\frac{r}{R_0}\right)}{log(\tau)}\right) \pm \delta \; with \; R_0 \leq r \leq R_0\tau^n$$

where $R_0$is the minimum radius of the antenna and depends on the greater frequency of interest, τ specifies the antenna profile periodicity, n is the number of the oscillations. Eventually, α is responsible of the amplitude of oscillations, while δ is the amplitude of the overshoots. Since the structure is printed on a substrate, electrical permittivity affects the overall dimensions.
The simulated models and dimensions of the radiating elements are shown in Figure 1.

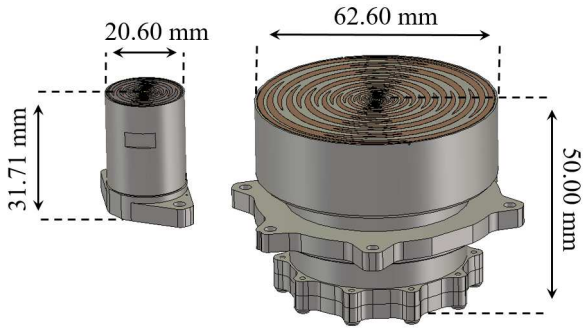

Figure 1. HB (left side) and LB (right side) antennas CAD model with dimensions.

Antennas have been manufactured using materials listed in Table 1. The comparison between free-space measurements and simulations performances are presented in [13].

Table 1. List of materials

Part	Material
Substrate	R5880
RF Absorber	MF 190
Cavity	Aluminum
Circuit	Copper

3 Interferometer Performance

The designed antennas have been assembled in the interferometric panel structure, as sketched in Figure 2. In this figure, the panel is installed in the near field facility setup OTA (Over The Air) TS8991 produced by Rohde&Schwarz [14]. The antennas has been placed according with the 2d–3d interferometric linear configuration.
The radiating performance have been elaborated with Matlab [15] in terms of reflection coefficient and boresight realized gain, as illustrated from Figure 3 to 6.

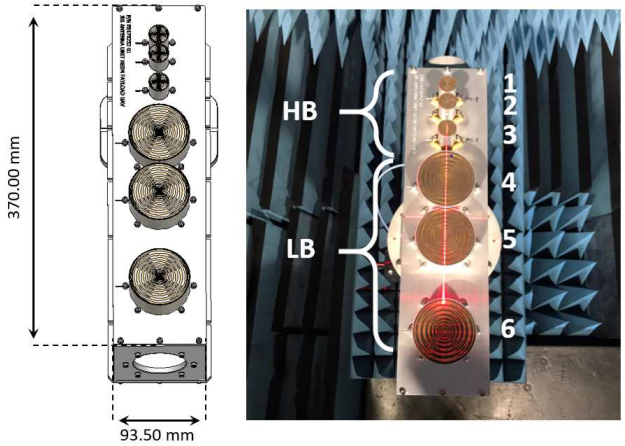

Figure 2. Interferometric panel dimensions and installation in the OTA.

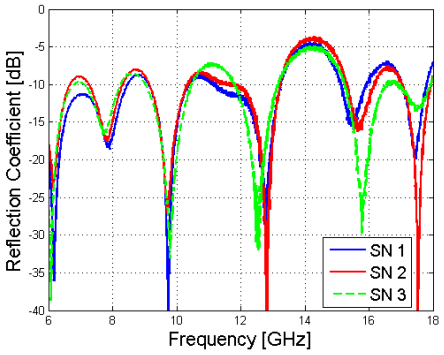

Figure 3. Reflection coefficient of the HB antennas. Numbering refers to Figure 2.

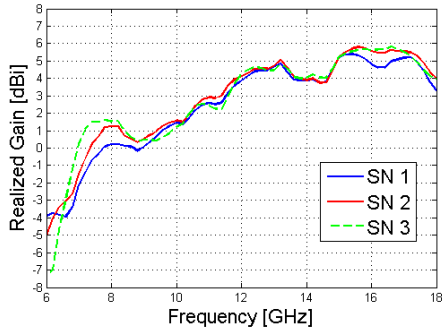

Figure 4. HB antenna boresight realized gain for the S45 polarization. Numbering refers to Figure 2.

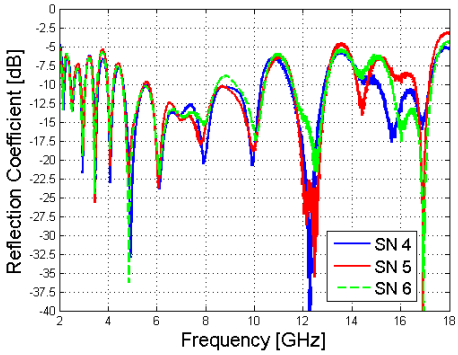

Figure 5. Reflection Coefficient of the LB antennas. Numbering refers to Figure 2.

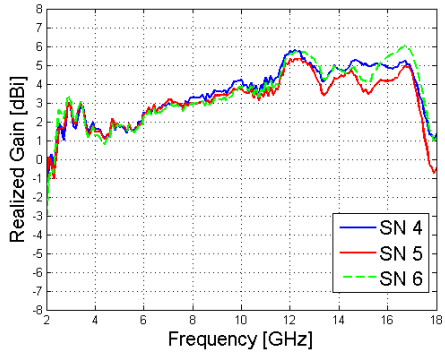

Figure 6. LB antenna boresight realized gain for the S45 polarization. Numbering refers to Figure 2.

The measured performance provide good matching properties of the two sets of sinuous antennas. Moreover, the measured boresight realized gain allow to achieve the desired sensitivity of the receiver. The final design of the proposed interferometric panel is shown in Figure 7. The measured overall weight is close to 1600g confirming the lightweight design approach.

Figure 7. Mockup of the POD with installed sinuous antennas.

4 Delta phase analysis

The interferometric panel works using the phase difference between a couple of antennas to estimates the azimuth direction of the RF source. For this reason, it is very important to characterize the radiated phase front of each antenna. Measures have been taken for each antenna keeping fixed the whole structure inside the NF measurement facility. The measured phase difference $\Delta\phi$ for each couple of antennas and for the S45 polarization has been compared with the expected theoretical phase values $\Delta\phi_{th}$ in order to evaluate the frequency behavior of the root mean square (RMS) of the phase error $\varepsilon_{\Delta\phi}^{RMS}$ on the azimuth-elevation plane. In particular, $\mathrm{Az} \times \mathrm{El} \in \left[-\frac{\Delta_{Az}}{2}, \frac{\Delta_{Az}}{2}\right] \times \left[-\frac{\Delta_{El}}{2}, \frac{\Delta_{El}}{2}\right]$, $\frac{\Delta_{Az}}{2} = 60°$ and $\frac{\Delta_{El}}{2} = 30°$.

$$\Delta\phi_{th}(Az, El) = \frac{2\pi}{\lambda} D \sin(Az)\cos(El)$$

$$\varepsilon_{\Delta\phi}^{RMS} = \sqrt{\frac{1}{\Delta_{Az}\Delta_{El}} \int_{-\Delta_{Az}/2}^{+\Delta_{Az}/2} \int_{-\Delta_{El}/2}^{+\Delta_{El}/2} \left(\Delta\phi(Az, El) - \Delta\phi_{th}(Az, El)\right)^2}$$

In Figure 8, the RMS phase error for each couple of antennas has been illustrated. The obtained results show a promising RMS error, except for the LB antennas at 2 GHz. In fact, around this frequency the mutual coupling plays a key role, since the antennas are electrically close.

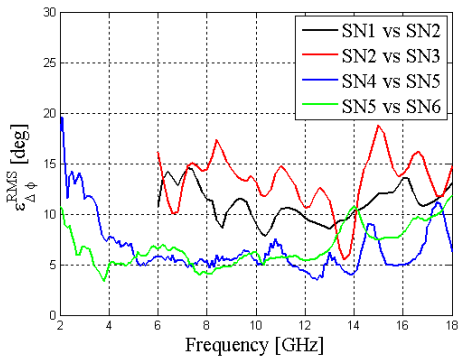

Figure 8. RMS of the delta phase error for each couple of antennas.

5 DoA Analysis

The DoA analysis performance has been carried out - for each sub-band of the interferometric panel – through the so-called sensitivity analysis of the Azimuth error which looks for the $\varepsilon_{\mathrm{Az}}$ consequent to the presence of some $\varepsilon_{\Delta\phi tot}$.

$$\Delta\phi_{th} + \varepsilon_{\Delta\phi tot} = \frac{2\pi \cdot D_{TOT}}{\lambda} \cdot \sin(Az + \varepsilon_{\mathrm{Az}})\cos(El) \cong \frac{2\pi \cdot D_{TOT}}{\lambda} \cdot \sin(Az)\cos(El) + \varepsilon_{\mathrm{Az}} \cdot \frac{2\pi \cdot D_{TOT}}{\lambda} \cdot \cos(Az)\cos(El)$$

where D_{TOT} represents the overall distance between antennas belonging to the propre sub-band. The random error $\varepsilon_{\mathrm{Az}}$ is so evaluated as:

$$\varepsilon(Az; El)_{\mathrm{Az}}^{RMS} \cong \frac{\lambda}{2\pi \cdot D_{TOT} \cdot cos(Az)\cos(El)} \cdot \varepsilon_{\Delta\phi tot}^{RMS}$$

In addiction it has to be considered that – since the interfermeter is purely linear – when $El \neq 0$ an additional error component (the so called "cone error") shall be present. The cone error cannot be treated as a random error being a deterministic function of an unknown parameter (e.g. the elevation):

$$\varepsilon_{cone}(Az, El) = asin(sin(Az)\, cos(El)) - Az$$

The overall RMS of the DoA error $\varepsilon_{\mathrm{Az}}^{RMS}$ is evaluated as:

$$\varepsilon(Az, El)_{\mathrm{ToT}}^{RMS} = \sqrt{[\varepsilon(Az; El)_{\mathrm{Az}}^{RMS}]^2 + [\varepsilon_{cone}(Az, El)]^2}$$

In Figure 9 it is illustrated the error estimation in the working frequency range averaged over the $[-60°, 60°]$ Az sector at Elevation 0°; cone error has not taken into account since, even if it affects the system performance, it is a purely geometric contribution, which does not have any relevance to electrical performances.

Performances have been shown in terms of both measured (continuous line) and theoretical (dotted line) data. The theoretical performances has been evaluated considering an uniform unbalances $\varepsilon_{\Delta\phi}^{RMS} = 10°$ in all the bandwidth. The results show an acceptable accuracy with a reduced performance only at 2 GHz where the phase unbalances generates an increasing DoA errors.

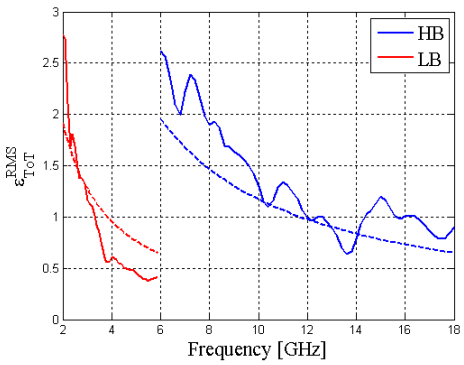

Figure 9. Error on azimuth direction estimation in the working frequency range with measured data (continuous line) and theoretical (dotted line).

6 Conclusions

In this paper, a very compact and lightweight interferometric panel for Direction Finding applications has been presented. Firstly, the radiating elements that compose the system have been designed and described. Then, the installed performances have been measured and eventually, the algorithm used to calculate the direction of arrival has been analyzed. The achieved DoA estimation performance are extremely good, confirming the effectiveness of the proposed solution.

7 References

1. Liu, L., Yu, T. "An Analysis Method for Solving Ambiguity in Direction Finding with Phase Interferometers". *Circuits Syst Signal Process (2020).* https://doi.org/10.1007/s00034-020-01536-1

2. L. Balogh and I. Kollar, "Angle of arrival estimation based on interferometer principle," *IEEE International Symposium on Intelligent Signal Processing*, 2003, Budapest, Hungary, 2003, pp. 219-223, doi: 10.1109/ISP.2003.1275842.

3. E. Jacobs and E. W. Ralston, "Ambiguity Resolution in Interferometry," *in IEEE Transactions on Aerospace and Electronic Systems*, vol. AES-17, no. 6, pp. 766-780, Nov. 1981, doi: 10.1109/TAES.1981.309127.

4. M. Gavish and A. J. Weiss, "Array geometry for ambiguity resolution in direction finding," *in IEEE Transactions on Antennas and Propagation*, vol. 44, no. 6, pp. 889-895, June 1996, doi: 10.1109/8.509893.

5. R.H. DuHamel. "Dual polarized sinuous antennas," *US Patent* 4,658,262. Apr. 1987.

6. Elettronica S.p.A. "Ultra-wide-band low-profile sinuous slot antenna array," *EP Patent* 2,629,367,B1. 2016.

7. S. Lizhong, C. Guojin, H. Huanfeng, "Simulation and analysis of a hemispherical conformal sinuous antenna with four arms," *Proc. IEEE Int. Conf. Ultra-Wideband (ICUWB)*, 2010, vol. 1, pp. 1–4.

8. A. Manna, P. Baldonero, F. Trotta, "Novel UWB lowprofile sinuous slot antenna," *Proc. 5th Eur. Conf. Antennas Propag. (EUCAP)*, 2011, pp. 783–786.

9. E. Agastra, L. Lucci, G. Pelosi, S. Selleri, "High gain compact strip and slot UWB sinuous antennas," *Int. J. Antennas Propag.* , vol. 2012, 9 pp., 2012.

10. L. Bartalucci, S. Maddio, G. Pelosi, M. Righini, L. Scorrano, S. Selleri, "A ultra wide band sinuous antenna design with enhanced linear polarization purity," *in 2019 URSI Asia-Pacific Radio Science Conference (AP-RASC)*, New Delhi (India), 09-15 March 2019, pp. 1–2.

11. C. M. Lamacchia et al., "Novel Miniaturized Sinuous Antenna for UWB Applications," *2020 XXXIIIrd General Assembly and Scientific Symposium of the International Union of Radio Science*, Rome, Italy, 2020, pp. 1-3, doi: 10.23919/URSIGASS49373.2020.9232245.

12. S. A. P. Rizvi and R. A. A. Khan, "Klopfenstein tapered 2–18 GHz microstrip balun," *Proceedings of 2012 9th International Bhurban Conference on Applied Sciences & Technology (IBCAST)*, Islamabad, 2012, pp. 359-362, doi: 10.1109/IBCAST.2012.6177579.

13. L. Scorrano et al., "A Compact and Lightweight Ultra-Wideband Interferometer for Direction Finding Applications," *2020 XXXIIIrd General Assembly and Scientific Symposium of the International Union of Radio Science*, Rome, Italy, 2020, pp. 1-4, doi: 10.23919/URSIGASS49373.2020.9232181.

14. https://www.rohde-schwarz.com/it/prodotto/ts8991-pagina-iniziale-delprodotto_63493-8444.html.

15. MATLAB. Natick, Massachusetts: The MathWorks Inc.